

Updated High-Temperature Opacities for The Dartmouth Stellar Evolution Program and their Effect on the Jao Gap Location

2 THOMAS M. BOUDREAUX¹ AND BRIAN C. CHABOYER¹

3 *¹Department of Physics and Astronomy, Dartmouth College, Hanover, NH 03755, USA*

4 ABSTRACT

5 The Jao Gap, a 17 percent decrease in stellar density at $M_G \sim 10$ identified in both Gaia DR2
6 and EDR3 data, presents a new method to probe the interior structure of stars near the fully con-
7 vective transition mass. The Gap is believed to originate from convective kissing instability wherein
8 asymmetric production of ^3He causes the core convective zone of a star to periodically expand and
9 contract and consequently the stars' luminosity to vary. Modeling of the Gap has revealed a sensitivity
10 in its magnitude to a population's metallicity primarily through opacity. Thus far, models of the Jao
11 Gap have relied on OPAL high-temperature radiative opacities. Here we present updated synthetic
12 population models tracing the Gap location modeled with the Dartmouth stellar evolution code using
13 the OPLIB high-temperature radiative opacities. Use of these updated opacities changes the predicted
14 location of the Jao Gap by ~ 0.05 mag as compared to models which use the OPAL opacities. This
15 difference is likely too small to be detectable in empirical data.

16 *Keywords:* Stellar Evolution (1599) — Stellar Evolutionary Models (2046)

17 1. INTRODUCTION

18 Due to the initial mass requirements of the molecular
19 clouds which collapse to form stars, star formation is
20 strongly biased towards lower mass, later spectral class
21 stars when compared to higher mass stars. Partly as
22 a result of this bias and partly as a result of their ex-
23 tremely long main-sequence lifetimes, M Dwarfs make
24 up approximately 70 percent of all stars in the galaxy.
25 Moreover, some planet search campaigns have focused
26 on M Dwarfs due to the relative ease of detecting small
27 planets in their habitable zones (e.g. Nutzman & Char-
28 bonneau 2008). M Dwarfs then represent both a key
29 component of the galactic stellar population as well as
30 the possible set of stars which may host habitable ex-
31 oplanets. Given this key location M Dwarfs occupy in
32 modern astronomy it is important to have a thorough
33 understanding of their structure and evolution.

34 Jao et al. (2018) discovered a novel feature in the Gaia
35 Data Release 2 (DR2) $G_{BP} - G_{RP}$ color-magnitude-
36 diagram. Around $M_G = 10$ there is an approximately

37 17 percent decrease in stellar density of the sample of
38 stars Jao et al. (2018) considered. Subsequently, this
39 has become known as either the Jao Gap, or Gaia M
40 Dwarf Gap. Following the initial detection of the Gap
41 in DR2 the Gap has also potentially been observed in
42 2MASS (Skrutskie et al. 2006; Jao et al. 2018); however,
43 the significance of this detection is quite weak and it re-
44 lies on the prior of the Gap's location from Gaia data.
45 Further, the Gap is also present in Gaia Early Data Re-
46 lease 3 (EDR3) (Jao & Feiden 2021). These EDR3 and
47 2MASS data sets then indicate that this feature is not
48 a bias inherent to DR2.

49 The Gap is generally attributed to convective instabil-
50 ities in the cores of stars straddling the fully convective
51 transition mass (0.3 - 0.35 M_\odot) (Baraffe & Chabrier
52 2018). These instabilities interrupt the normal, slow,
53 main sequence luminosity evolution of a star and result
54 in luminosities lower than expected from the main se-
55 quence mass-luminosity relation (Jao & Feiden 2020).

56 The Jao Gap, inherently a feature of M Dwarf pop-
57 ulations, provides an enticing and unique view into the
58 interior physics of these stars (Feiden et al. 2021). This
59 is especially important as, unlike more massive stars,
60 M Dwarf seismology is infeasible due to the short peri-
61 ods and extremely small magnitudes which both radial
62 and low-order low-degree non-radial seismic waves are

Corresponding author: Thomas M. Boudreax
thomas.m.boudreaux.gr@dartmouth.edu,
thomas@boudreauxmail.com

⁶³ predicted to have in such low mass stars (Rodríguez-
⁶⁴ López 2019). The Jao Gap therefore provides one of the
⁶⁵ only current methods to probe the interior physics of M
⁶⁶ Dwarfs.

⁶⁷ Despite the early success of modeling the Gap some
⁶⁸ issues remain. Jao & Feiden (2020, 2021) identify that
⁶⁹ the Gap has a wedge shape which has not been successful
⁷⁰ reproduced by any current modeling efforts and which
⁷¹ implies a somewhat unusual population composition of
⁷² young, metal-poor stars. Further, Jao & Feiden (2020)
⁷³ identify substructure, an additional over density of stars,
⁷⁴ directly below the Gap, again a feature not yet fully
⁷⁵ captured by current models.

⁷⁶ All currently published models of the Jao Gap make
⁷⁷ use of OPAL high temperature radiative opacities. Here
⁷⁸ we investigate the effect of using the more up-to-
⁷⁹ date OPLIB high temperature radiative opacities and
⁸⁰ whether these opacity tables bring models more in line
⁸¹ with observations. In Section 2 we provide an overview
⁸² of the physics believed to result in the Jao Gap, in
⁸³ Section 3 we review the differences between OPAL
⁸⁴ and OPLIB and describe how we update DSEP to use
⁸⁵ OPLIB opacity tables. Section 4 walks through the stel-
⁸⁶ lar evolution and population synthesis modeling we per-
⁸⁷ form. Finally, in Section 5 we present our findings.

2. JAO GAP

⁸⁸ A theoretical explanation for the Jao Gap (Figure 1)
⁸⁹ comes from van Saders & Pinsonneault (2012), who pro-
⁹⁰ pose that in a star directly above the transition mass,
⁹¹ due to asymmetric production and destruction of ^3He
⁹² during the proton-proton I chain (ppI), periodic lumi-
⁹³ nosity variations can be induced. This process is known
⁹⁴ as convective-kissing instability. Very shortly after the
⁹⁵ zero-age main sequence such a star will briefly develop
⁹⁶ a radiative core; however, as the core temperature ex-
⁹⁷ ceeds 7×10^6 K, enough energy will be produced by the
⁹⁸ ppI chain that the core once again becomes convective.
⁹⁹ At this point the star exists with both a convective core
¹⁰⁰ and envelope, in addition to a thin, radiative layer sepa-
¹⁰¹ rating the two. Subsequently, asymmetries in ppI affect
¹⁰² the evolution of the star’s convective core.

¹⁰³ While kissing instability has been the most widely
¹⁰⁴ adopted model to explain the existence of the Jao Gap,
¹⁰⁵ slightly different mechanisms have also been proposed.
¹⁰⁶ MacDonald & Gizis (2018) make use of a fully implicit
¹⁰⁷ stellar evolution suite which treats convective mixing
¹⁰⁸ as a diffusive property. MacDonald & Gizis treat con-
¹⁰⁹ vective mixing this way in order to account for a core
¹¹⁰ deuterium concentration gradient proposed by Baraffe
¹¹¹ et al. (1997). Under this treatment the instability re-
¹¹²sults only in a single mixing event — as opposed to pe-

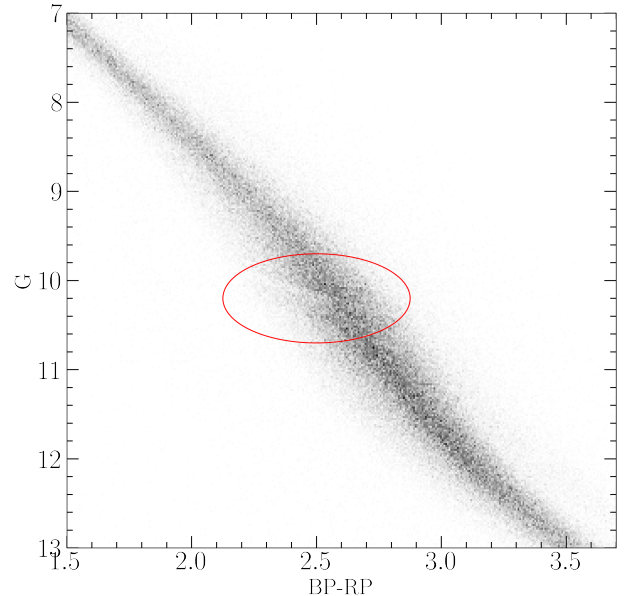


Figure 1. The Jao Gap (circled) seen in the Gaia Catalogue of Nearby Stars (Gaia Collaboration et al. 2021).

¹¹⁴ riodic mixing events. Single mixing events may be more
¹¹⁵ in line with observations (see section 5 for more details
¹¹⁶ on how periodic mixings can effect a synthetic popula-
¹¹⁷ tion) where there is only well documented evidence of
¹¹⁸ a single gap. However, recent work by Jao & Feiden
¹¹⁹ (2021) which identify an second under density of stars
¹²⁰ below the canonical gap, does leave the door open for
¹²¹ the periodic mixing events.

¹²² The proton-proton I chain constitutes three reactions

- ¹²³ 1. $p + p \rightarrow d + e^+ + \nu_e$
- ¹²⁴ 2. $p + d \rightarrow ^3\text{He} + \gamma$
- ¹²⁵ 3. $^3\text{He} + ^3\text{He} \rightarrow ^3\text{He} + 2p$

¹²⁶ Initially, reaction 3 of ppI consumes ^3He at a slower
¹²⁷ rate than it is produced by reaction 2 and as a result,
¹²⁸ the core ^3He abundance and consequently the rate of
¹²⁹ reaction 3, increases with time. The core convective
¹³⁰ zone expands as more of the star becomes unstable to
¹³¹ convection. This expansion continues until the core con-
¹³²nects with the convective envelope. At this point convec-
¹³³tive mixing can transport material throughout the entire
¹³⁴ star and the high concentration of ^3He rapidly diffuses
¹³⁵ outward, away from the core, decreasing energy genera-
¹³⁶tion as reaction 3 slows down. Ultimately, this leads to
¹³⁷ the convective region around the core pulling back away
¹³⁸ from the convective envelope, leaving in place the radi-
¹³⁹ative transition zone, at which point ^3He concentrations
¹⁴⁰ grow in the core until it once again expands to meet
¹⁴¹ the envelope. These periodic mixing events will con-
¹⁴²tinue until ^3He concentrations throughout the star reach

an equilibrium ultimately resulting in a fully convective star. Figure 2 traces the evolution of a characteristic star within the Jao Gap’s mass range.

2.1. Efforts to Model the Gap

Since the identification of the Gap, stellar modeling has been conducted to better constrain its location, effects, and exact cause. Both Mansfield & Kroupa (2021) and Feiden et al. (2021) identify that the Gap’s mass location is correlated with model metallicity — the mass-luminosity discontinuity in lower metallicity models being at a commensurately lower mass. Feiden et al. (2021) suggests this dependence is due to the steep relation of the radiative temperature gradient, ∇_{rad} , on temperature and, in turn, on stellar mass.

$$\nabla_{rad} \propto \frac{L\kappa}{T^4} \quad (1)$$

As metallicity decreases so does opacity, which, by Equation 1, dramatically lowers the temperature at which radiation will dominate energy transport (Chabrier & Baraffe 1997). Since main sequence stars are virialized the core temperature is proportional to the core density and total mass. Therefore, if the core temperature where convective-kissing instability is expected decreases with metallicity, so too will the mass of stars which experience such instabilities.

The strong opacity dependence of the Jao Gap begs the question: **what is the effect of different opacity calculations on Gap properties**. As we can see above, changing opacity should affect the Gap’s location in the mass-luminosity relation and therefore in a color-magnitude diagram. Moreover, current models of the Gap have yet to locate it precisely in the CMD (Feiden et al. 2021) with an approximate 0.16 G-magnitude difference between the observed and modeled Gaps. Opacity provides one, as yet unexplored, parameter which has the potential to resolve these discrepancies.

3. UPDATED OPACITIES

Multiple groups have released high-temperature opacities including, the Opacity Project (OP Seaton et al. 1994), Lawrence Livermore National Labs OPAL opacity tables (Iglesias & Rogers 1996), and Los Alamos National Labs OPLIB opacity tables (Colgan et al. 2016). OPAL high-temperature radiative opacity tables in particular are very widely used by current generation isochrone grids (e.g. Dartmouth, MIST, & StarEvol, Dotter et al. 2008; Choi et al. 2016; Amard et al. 2019). OPLIB opacity tables (Colgan et al. 2016) are not widely used but include the most up-to-date plasma modeling.

While the overall effect on the CMD of using OPLIB compared to OPAL tables is small, the strong theoretical opacity dependence of the Jao Gap raises the potential for these small effects to measurably shift the Gap’s location. We update DSEP to use high temperature opacity tables based on measurements from Los Alamos national Labs T-1 group (OPLIB, Colgan et al. 2016). The OPLIB tables are created with ATOMIC (Magee et al. 2004; Hakel et al. 2006; Fontes et al. 2015), a modern LTE and non-LTE opacity and plasma modeling code. These updated tables were initially created in order to incorporate the most up to date plasma physics at the time (Bahcall et al. 2005).

OPLIB tables include monochromatic Rosseland mean opacities — composed from bound-bound, bound-free, free-free, and scattering opacities — for elements hydrogen through zinc over temperatures 0.5eV to 100 keV ($5802\text{ K} - 1.16 \times 10^9\text{ K}$) and for mass densities from approximately 10^{-8} g cm^{-3} up to approximately 10^4 g cm^{-3} (though the exact mass density range varies as a function of temperature).

DSEP ramps the Ferguson et al. (2005) low temperature opacities to high temperature opacities tables between $10^{4.3}\text{ K}$ and $10^{4.5}\text{ K}$; therefore, only differences between high-temperature opacity sources above $10^{4.3}\text{ K}$ can effect model evolution. When comparing OPAL and OPLIB opacity tables (Figure 3) we find OPLIB opacities are systematically lower than OPAL opacities for temperatures above 10^5 K . Between $10^{4.3}$ and 10^5 K OPLIB opacities are larger than OPAL opacities. These generally lower opacities will decrease the radiative temperature gradient throughout much of the radius of a model.

3.1. Table Querying and Conversion

The high-temperature opacity tables used by DSEP and most other stellar evolution programs give Rosseland-mean opacity, κ_R , along three dimensions: temperature, a density proxy R (Equation 2; $T_6 = T \times 10^{-6}$, ρ is the mass density), and composition.

$$R = \frac{\rho}{T_6^3} \quad (2)$$

OPLIB tables may be queried from a web interface¹; however, OPLIB opacities are parametrized using mass-density and temperature instead of R and temperature. It is most efficient for us to convert these tables to the OPAL format instead of modifying DSEP to use the OPLIB format directly. In order to generate

¹ <https://aphysics2.lanl.gov/apps/>

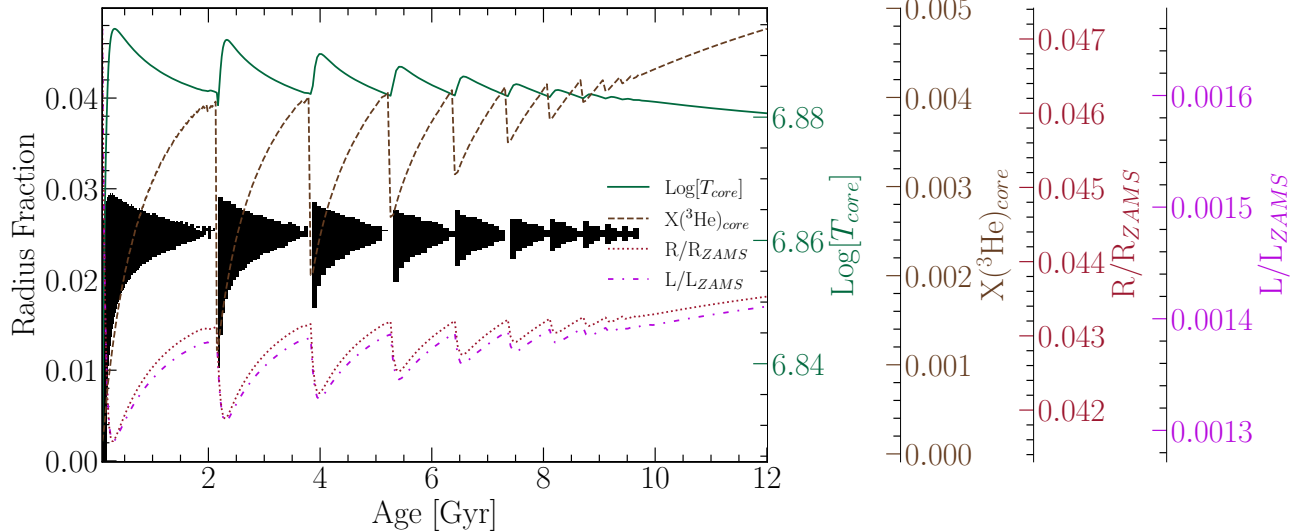


Figure 2. Diagram for a characteristic stellar model of $0.35625 M_{\odot}$ which is within the Jao Gap’s mass range. The black shaded regions denote whether, at a particular model age, a radial shell within the model is radiative (with white meaning convective). The lines trace the models core temperature, core ${}^3\text{He}$ mass fraction, fractional luminosity wrt. the zero age main sequence and fractional radius wrt. the zero age main sequence.

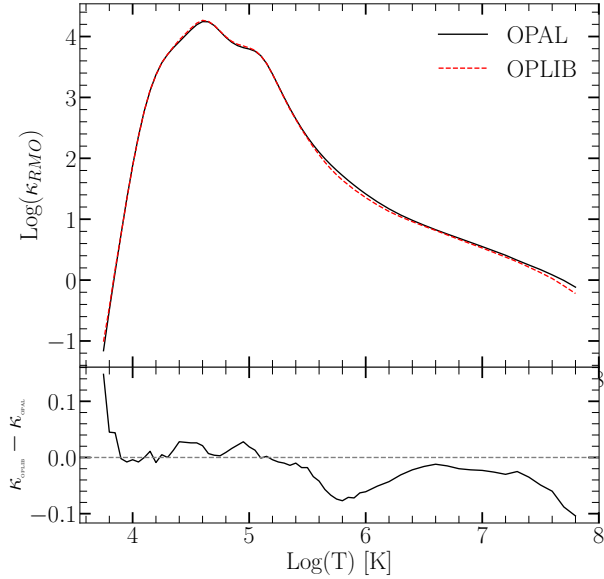


Figure 3. Rosseland mean opacity with the GS98 solar composition for both OPAL opacities and OPLIB opacities (top). Residuals between OPLIB opacities and OPAL opacities (bottom). These opacities are plotted at $\log_{10}(R) = -0.5$, $X = 0.7$, and $Z = 0.02$. $\log_{10}(R) = -0.5$ approximates much of the interior a $0.35 M_{\odot}$ model. Note how the OPLIB opacities are systematically lower than the OPAL opacities for temperatures above $10^{5.2}$ K.

many tables easily and quickly we develop a web scraper (pyTOPSScrape, Boudreaux 2022) which can automatically retrieve all the tables needed to build an opacity

table in the OPAL format. pyTOPSScrape² has been released under the permissive MIT license with the consent of the Los Alamos T-1 group. For a detailed discussion of how the web scraper works and how OPLIB tables are transformed into a format DSEP can use see Appendices A & B.

3.2. Solar Calibrated Stellar Models

In order to validate the OPLIB opacities, we generated a solar calibrated stellar model (SCSM) using these new tables. We first manually calibrate the surface Z/X abundance to within one part in 100 of the solar value (Grevesse & Sauval 1998, $Z/X=0.23$). Subsequently, we allow both the convective mixing length parameter, α_{ML} , and the initial Hydrogen mass fraction, X , to vary simultaneously, minimizing the difference, to within one part in 10^5 , between resultant models’ final radius and luminosity to those of the sun. Finally, we confirm that the model’s surface Z/X abundance is still within one part in 100 of the solar value.

Solar calibrated stellar models evolved using GS98 OPAL and OPLIB opacity tables (Figure 4) differ $\sim 0.5\%$ in the SCSM hydrogen mass fractions and $\sim 1.5\%$ in the SCSM convective mixing length parameters (Table 1). While the two evolutionary tracks are very similar, note that the OPLIB SCSM’s luminosity is systematically lower past the solar age. While at the solar age the OPLIB SCSM luminosity is effectively the same as the OPAL SCSM. This luminosity difference between

² <https://github.com/tboudreaux/pytopsscrape>

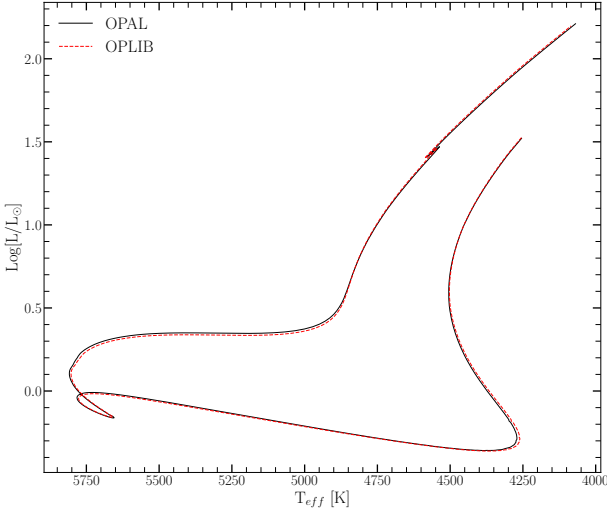


Figure 4. HR Diagram for the two SCSMs, OPAL and OPLIB. OPLIB is shown as a red dashed line.

Model	X	α_{ML}
OPAL	0.7066	1.9333
OPLIB	0.7107	1.9629

Table 1. Optimized parameters for SCSMs evolved using OPAL and OPLIB high temperature opacity tables.

OPAL and OPLIB based models is not inconsistent with expectations given the more shallow radiative temperature gradient resulting from the lower OPLIB opacities

4. MODELING

In order to model the Jao Gap we evolve two extremely finely sampled mass grids of models. One of these grids uses the OPAL high-temperature opacity tables while the other uses the OPLIB tables (Figure 5). Each grid evolves a model every $0.00025 M_\odot$ from 0.2 to $0.4 M_\odot$ and every $0.005 M_\odot$ from 0.4 to $0.8 M_\odot$. All models in both grids use a GS98 solar composition, the (1, 101, 0) FreeEOS (version 2.7) configuration, and 1000 year old pre-main sequence polytropic models, with polytropic index 1.5, as their initial conditions. We include gravitational settling in our models where elements are grouped together. Finally, we set a maximum allowed timestep of 50 million years to assure that we fully resolve the build of of core ^3He in gap stars.

Despite the alternative view of convection provided by MacDonald & Gizis (2018) discussed in Section 2, given that the mixing timescales in these low mass stars are so short (between 10^7 s and 10^8 s per Jermyn et al. 2022, Figure 2 & Equation 39, which present the averaged velocity over the convection zone) instantaneous mixing is a valid approximation. Moreover, one principal motivation for a diffusive model of convec-

tive mixing has been to account for a deuterium concentration gradient which Chabrier & Baraffe (1997) identify will develop when the deuterium lifetime against proton capture is significantly shorter than the mixing timescale. However, the treatment of energy generation used by DSEP (Bahcall et al. 2001) avoids this issue by computing both the equilibrium deuterium abundance and luminosity of each shell individually, implicitly accounting for the overall luminosity discrepancy identified by Chabrier & Baraffe.

Because in this work we are just interested in the location shift of the Gap as the opacity source varies, we do not model variations in composition. Mansfield & Kroupa (2021); Jao & Feiden (2020); Feiden et al. (2021) all look at the effect composition has on Jao Gap location. They find that as population metallicity increases so too does the mass range and consequently the magnitude of the Gap. From an extremely low metallicity population ($Z=0.001$) to a population with a more solar like metallicity this shift in mass range can be up to $0.05 M_\odot$ (Mansfield & Kroupa 2021).

4.1. Population Synthesis

In order to compare the Gap to observations we use in house population synthesis code. We empirically calibrate the relation between G, BP, and RP magnitudes and their uncertainties along with the parallax/G magnitude uncertainty relation using the Gaia Catalogue of Nearby Stars (GCNS, Gaia Collaboration et al. 2021) and Equations 3 & 4. M_g is the Gaia G magnitude while M_i is the magnitude in the i^{th} band, G, BP, or RP. The coefficients a , b , and c determined using a non-linear least squares fitting routine. Equation 3 then models the relation between G magnitude and parallax uncertainty while Equation 4 models the relation between each magnitude and its uncertainty.

$$\sigma_{plx}(M_g) = ae^{bM_g} + c \quad (3)$$

$$\sigma_i(M_i) = ae^{M_i - b} + c \quad (4)$$

The full series of steps in our population synthesis code are:

1. Sample from a Sollima (2019) ($0.25M_\odot < M < 1M_\odot$, $\alpha = -1.34 \pm 0.07$) IMF to determine synthetic star mass.
2. Find the closest model above and below the synthetic star, linearly interpolate these models' T_{eff} , $\log(g)$, and $\log(L)$ to those at the synthetic star mass.

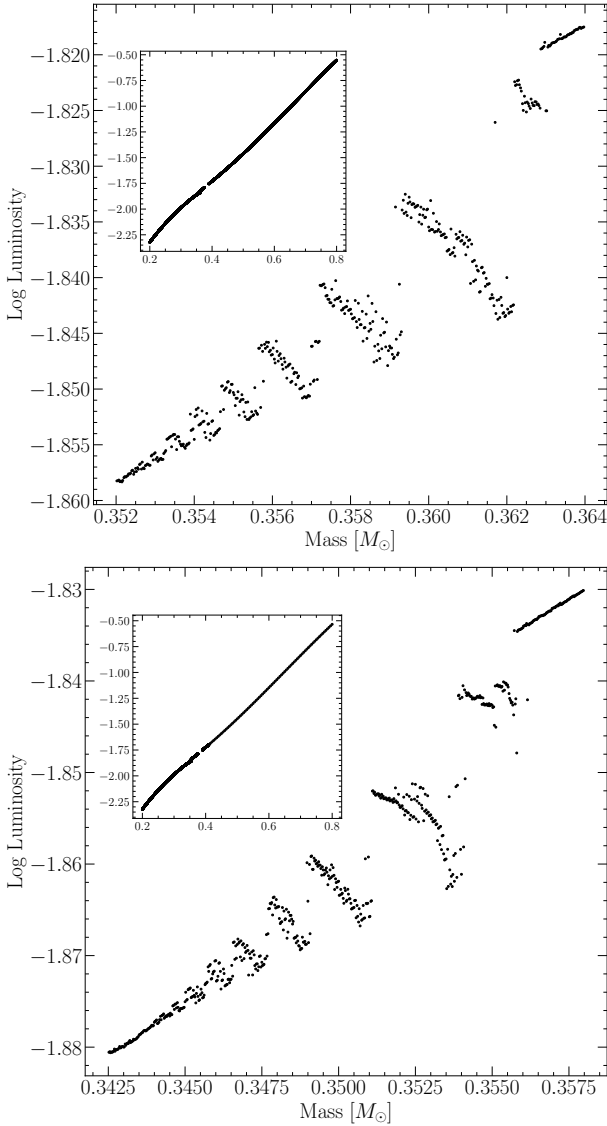


Figure 5. Mass-luminosity relation at 7 Gyrs for models evolved using OPAL opacity tables (top) and those evolved using OPLIB opacity tables (bottom). Note the lower mass range of the OPLIB Gap.

- 344 3. Convert synthetic star g , T_{eff} , and $\text{Log}(L)$ to Gaia
345 G, BP, and RP magnitudes using the Gaia (E)DR3
346 bolometric corrections (Creevey et al. 2022) along
347 with code obtained thorough personal communication
348 with Aaron Dotter (Choi et al. 2016).
- 349 4. Sample from the GCNS parallax distribution (Figure 350 6), limited to stars within the BP-RP color
351 range of 2.3 – 2.9, to assign synthetic star a “true”
352 parallax.
- 353 5. Use the true parallax to find an apparent magnitude
354 for each filter.

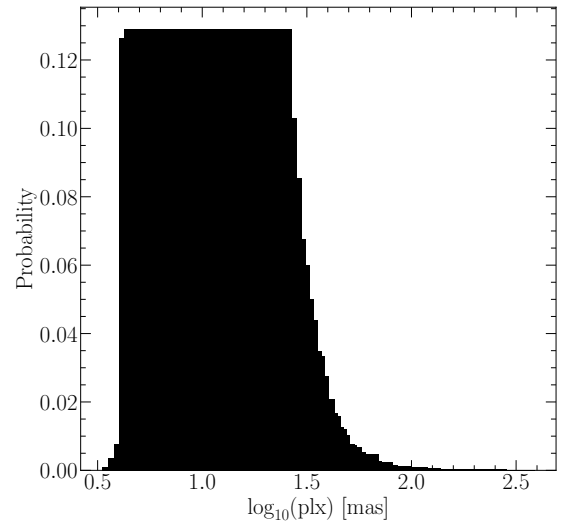


Figure 6. Probability distribution sampled when assigning true parallaxes to synthetic stars. This distribution is built from the GCNS and includes all stars with BP-RP colors between 2.3 and 2.9, the same color range of the Jao Gap.

- 355 6. Evaluate the empirical calibration given in Equation
356 3 to find an associated parallax uncertainty.
357 Then sample from a normal distribution with a
358 standard deviation equal to that uncertainty to
359 adjust the true parallax resulting in an “observed”
360 parallax.
- 361 7. Use the “observed” parallax and the apparent
362 magnitude to find an “observed” magnitude.
- 363 8. Fit the empirical calibration given in Equation 4
364 to the GCNS and evaluate it to give a magnitude
365 uncertainty scale in each band.
- 366 9. Adjust each magnitude by an amount sampled
367 from a normal distribution with a standard devi-
368 ation of the magnitude uncertainty scale found
369 in the previous step.

370 This method then incorporates both photometric and
371 astrometric uncertainties into our population synthe-
372 sis. An example 7 Gyr old synthetic populations using
373 OPAL and OPLIB opacities are presented in Figure 7.

374 4.2. Mixing Length Dependence

375 In order to test the sensitivity of Gap properties to
376 mixing length we evolve three separate sets OPLIB of
377 models. The first uses a GS98 solar calibrated mixing
378 length, the second uses a mixing length of 1.5, and the
379 third uses a mixing length of 1.0.

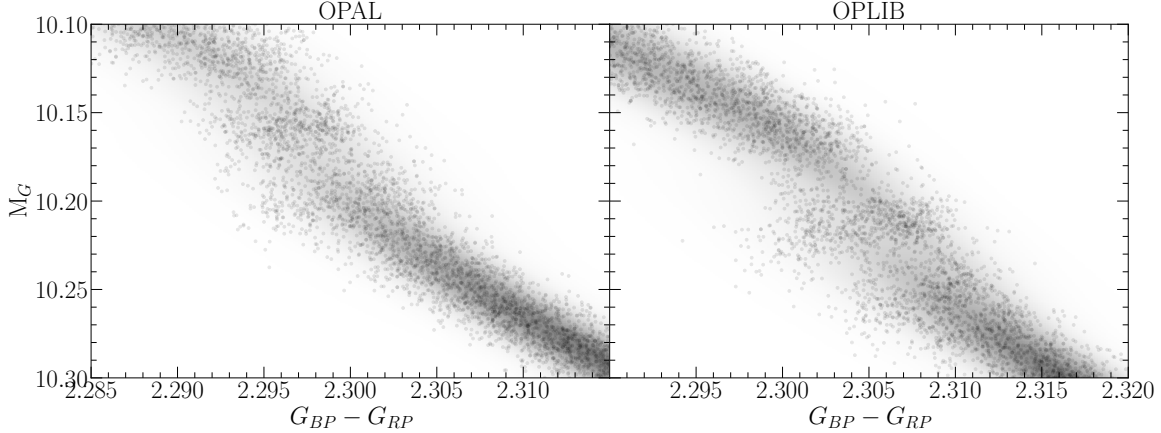


Figure 7. Population synthesis results for models evolved with OPAL (left) and models evolved with OPLIB (right). A Gaussian kernel-density estimate has been overlaid to better highlight the density variations.

We find a clear inverse correlation between mixing length parameter used and the magnitude of the Jao Gap Figures 8 & 9 ($\mu_G \propto -1.5\alpha_{ML}$, where μ_G is the mean magnitude of the Gap). This is somewhat surprising given the long established view that the mixing length parameter is of little relevance in fully convective stars (Baraffe et al. 1997). We find an approximate 0.3 magnitude shift in both the color and magnitude comparing a solar calibrated mixing length to a mixing length of 1.5, despite only a 16K difference in effective temperature at 7Gyr between two 0.3 solar mass models. **The slight temperature differences between these models are attributable to the steeper adiabatic temperature gradients just below the atmosphere in the solar calibrated mixing length model compared to the $\alpha_{ML} = 1.5$ model ($\nabla_{ad,solar} - \nabla_{ad,1.5} \approx 0.05$).** Despite this relatively small temperature variance, the large magnitude difference is expected due to the extreme sensitivity of the bolometric corrections on effective temperature at these low temperatures. The mixing length then provides a free parameter which may be used to shift the gap location in order to better match observations without having a major impact on the effective temperature of models. Moreover, recent work indicates that using a solar calibrated mixing length is not appropriate for all stars (e.g. Trampedach et al. 2014; Joyce & Chaboyer 2018).

Given the variability of gap location with mixing length, it is possible that a better fit to the gap location may be achieved through adjustment of the convective mixing length parameter. However, calibrations of the mixing length for stars other than the sun have focused on stars with effective temperature at or above that of the sun and there are no current calibrations of the mixing length parameter for M dwarfs. Moreover,

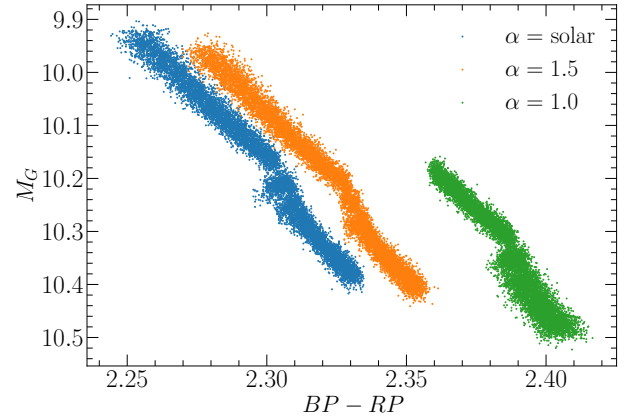


Figure 8. CMD showing OPLIB populations (from left to right) A, B, and C.

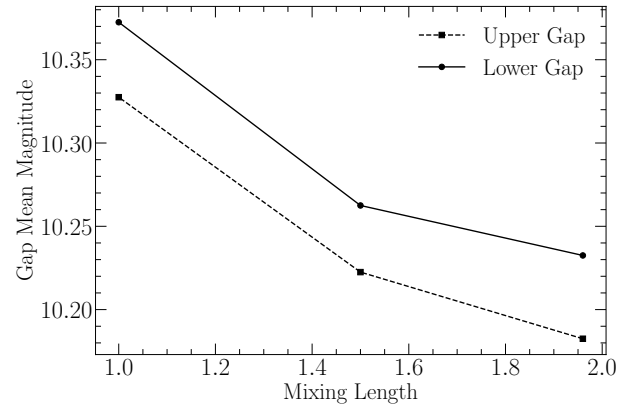


Figure 9. Location of the two identified paucities of stars in OPLIB synthetic populations as a function of the mixing length used.

there are additional uncertainties when comparing the predicted gap location to the measured gap location, such as those in the conversion from effective temper-

Model	Location	Prominence	Width
OPAL 1	10.138	0.593	0.027
OPAL 2	10.183	0.529	0.023
OPLIB 1	10.188	0.724	0.032
OPLIB 2	10.233	0.386	0.027

Table 2. Locations identified as potential Gaps.

ature, surface gravity, and luminosity to color, which must be considered if the mixing length is to be used as a gap location free parameter. Given the dangers of freely adjustable parameters and the lack of an a priori expectation for what the convective mixing parameter should be for the population of M Dwarfs in the Gaia DR2 and EDR3 CMD any attempt to use the Jao Gap magnitude to calibrate a mixing length value must be done with caution, and take into account the other uncertainties in the stellar models which could affect the Jao Gap magnitude.

5. RESULTS

We quantify the Jao Gap location along the magnitude (Table 2) axis by sub-sampling our synthetic populations, finding the linear number density along the magnitude axis of each sub-sample, averaging these linear number densities, and extracting any peaks above a prominence threshold of 0.1 as potential magnitudes of the Jao Gap (Figure 10). Gap widths are measured at 50% the height of the peak prominence. We use the python package `scipy` (Virtanen et al. 2020) to both identify peaks and measure their widths.

In both OPAL and OPLIB synthetic populations our Gap identification method finds two gaps above the prominence threshold. The identification of more than one gap is not inconsistent with the mass-luminosity relation seen in the grids we evolve. As noise is injected into a synthetic population smaller features will be smeared out while larger ones will tend to persist. The mass-luminosity relations shown in Figure 5 make it clear that there are: (1), multiple gaps due to stars of different masses undergoing convective mixing events at different ages, and (2), the gaps decrease in width moving to lower masses / redder. Therefore, the multiple gaps we identify are attributable to the two bluest gaps being wide enough to not smear out with noise. In fact, if we lower the prominence threshold just slightly from 0.1 to 0.09 we detect a third gap in both the OPAL and OPLIB datasets where one would be expected.

Previous modeling efforts (e.g. Feiden et al. 2021) have not identified multiple gaps. This is likely due to two reasons: (1), previous studies have allowed metallicity to vary across their model grids, further smearing the gaps

out, and (2), previous studies have used more coarse underlying mass grids, obscuring features smaller than their mass step. While this dual-gap structure has not been seen in models before, a more complex gap structure is not totally unprecedented as Jao & Feiden (2021) identifies an additional under-dense region below the primary gap in EDR3 data. As part of a follow up series of papers, we are conducting further work to incorporate metallicity variations while still using the finer mass sampling presented here.

The mean gap location of the OPLIB population is at a fainter magnitude than the mean gap location of the OPAL population. Consequently, in the OPLIB sample the convective mixing events which drive the kissing instability begin happening at lower masses (i.e. the convective transition mass decreases). A lower mass range will naturally result in a fainter mean gap magnitude.

Mixing events at lower masses in OPLIB models are attributable to the radially thicker, at the same mass, radiative zones (Figure 11). This thicker radiative zone will take more time to break down and is characteristic of OPLIB models as of a result of their slightly lower opacities. A lower opacity fluid will have a more shallow radiative temperature gradient than a higher opacity fluid; however, as the adiabatic temperature gradient remains essentially unchanged as a function of radius, a larger interior radius of the model will remain unstable to radiation. This thicker radiative zone will increase the time it takes the core convective zone to meet up with convective envelope meaning that lower mass models can sustain a radiative zone for longer than they could otherwise; thus; lower opacities push the convective transition mass down. We can additionally see this longer lived radiative zone in the core ^3He mass fraction, in which OPLIB models reach much higher concentrations — at approximately the same growth rate — for the same mass as OPAL models do (Figure 12).

The most precise published Gap location comes from Jao & Feiden (2020) who use EDR3 to locate the Gap at $M_G \sim 10.3$, we identify the Gap at a similar location in the GCNS data. **The Gap in populations evolved using OPLIB tables is closer to this measurement than it is in populations evolved using OPAL tables (Table 2).** It should be noted that the exact location of the observed Gap is poorly captured by a single value as the Gap visibly compresses across the width of the main-sequence, wider on the blue edge and narrower on the red edge such that the observed Gap has downward facing a wedge shape (Figure 1). This wedge shape is not successfully reproduced by either any current models or the modeling we perform here. We elect

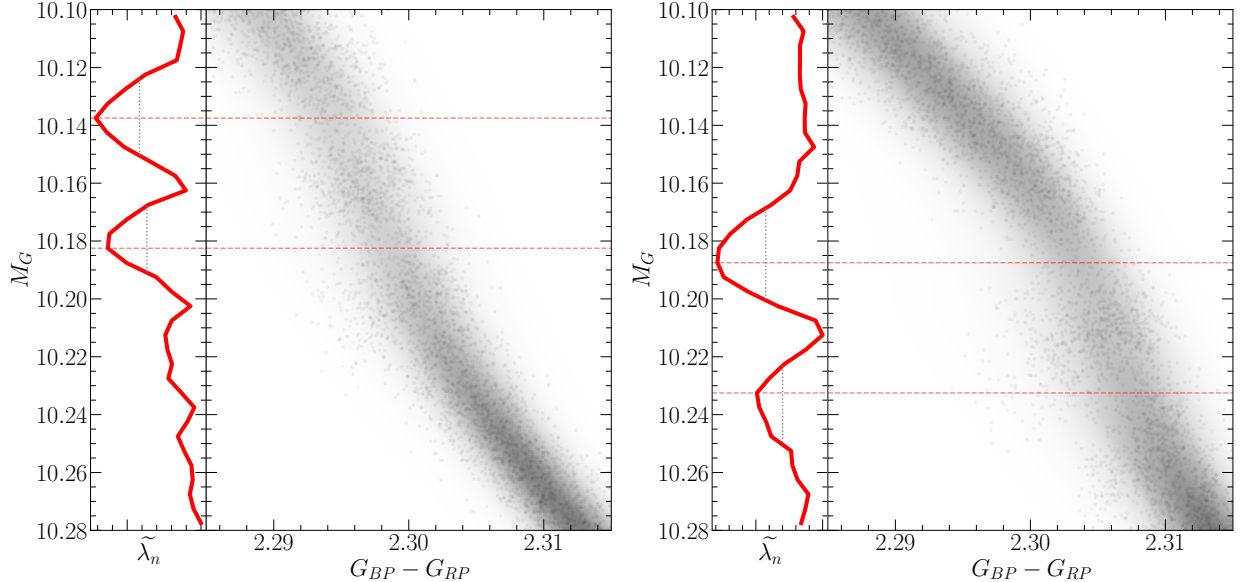


Figure 10. (right panels) OPAL (left) and OPLIB (right) synthetic populations. (left panels) Normalized linear number density along the magnitude axis. A dashed line has been extended from the peak through both panels to make clear where the identified Jao Gap location is wrt. to the population.

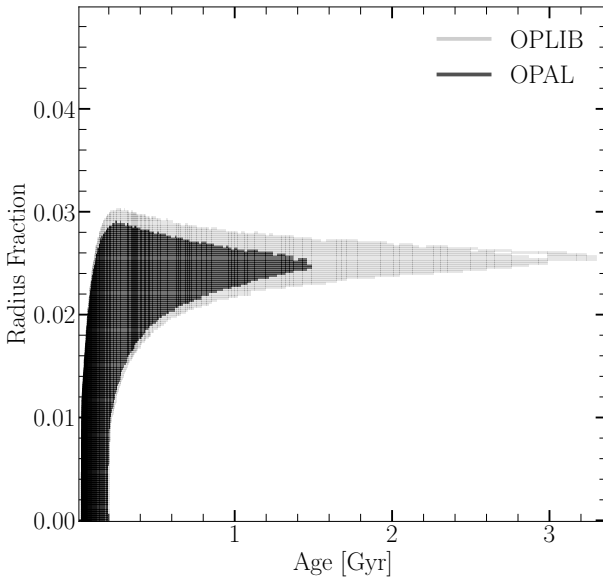


Figure 11. Portions of $0.3526 M_{\odot}$ OPAL and OPLIB stellar models showing the interior shells which are radiative (black region). Note that for clarity only one convective mixing event from each model is shown. Note how the radiative zone in the OPLIB model is larger.

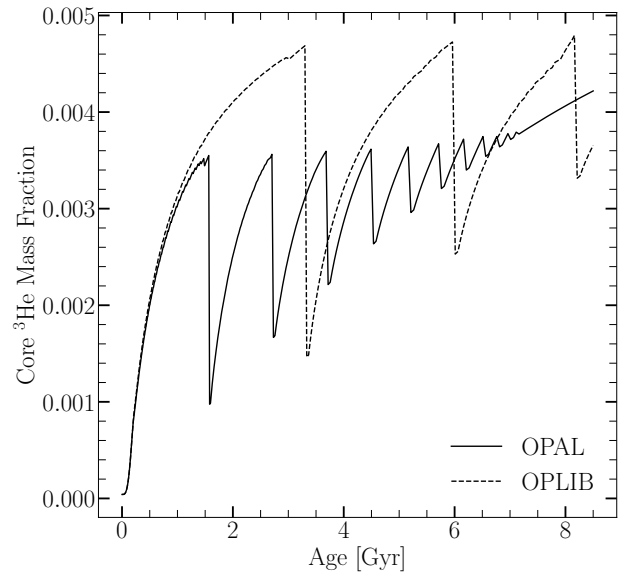


Figure 12. Core ${}^3\text{He}$ mass fraction for $0.3526 M_{\odot}$ models evolved with OPAL and OPLIB (within the Jao Gap's mass range for both). Note how the OPLIB model's core ${}^3\text{He}$ mass fraction grows at approximately the same rate as the OPAL model's but continues uninterrupted for longer.

then to specify the Gap location where this wedge is at its narrowest, on the red edge of the main sequence.

The Gaps identified in our modeling have widths of approximately 0.03 magnitudes, while the shift from OPAL to OPLIB opacities is 0.05 magnitudes. With the prior that the Gaps clearly shift before noise is injected we know that this shift is real. However, the

shift magnitude and Gap width are of approximately the same size in our synthetic populations. Moreover, Feiden et al. (2021) identify that the shift in the modelled Gap mass from $[\text{Fe}/\text{H}] = 0$ to $[\text{Fe}/\text{H}] = +0.5$ as $0.04 M_{\odot}$, whereas we only see an approximate $0.01 M_{\odot}$ shift between OPAL and OPLIB models. Therefore,

526 the Gap location will likely not provide a usable
 527 constraint on the opacity source.

528 6. CONCLUSION

529 The Jao Gap provides an intriguing probe into the in-
 530 terior physics of M Dwarfs stars where traditional meth-
 531 ods of studying interiors break down. However, before
 532 detailed physics may be inferred it is essential to have
 533 models which are well matched to observations. Here
 534 we investigate whether the OPLIB opacity tables repro-
 535 duce the Jao Gap location and structure more accurately
 536 than the widely used OPAL opacity tables. We find that
 537 while the OPLIB tables do shift the Jao Gap location
 538 more in line with observations, by approximately 0.05
 539 magnitudes, the shift is small enough that it is likely
 540 not distinguishable from noise due to population age
 541 and chemical variation. However, future measurement
 542 of [Fe/H] for stars within the gap will be helpful in con-
 543 straining the degree to which the gap should be smeared
 544 by these theoretical models.

545 We also find that both the color and magnitude of the
 546 Jao Gap are correlated to the convective mixing length

547 parameter. Specifically, a lower mixing length param-
 548 eter will bring the gap in the populations presented in
 549 this paper more in line with the current best estimate
 550 for the actual gap magnitude. Using this relation it may
 551 be possible for mixing length to be calibrated for low
 552 mass stars such that models match the Jao Gap loca-
 553 tion. Further, the Jao gap location may provide a test of
 554 alternative convection models such as entropy calibrated
 555 convection (Spada et al. 2021). Both of these potential
 556 uses require careful handeling of other uncertainties such
 557 as the uncertainties in bolometric correction, popula-
 558 tion composition, and population age. As we currently
 559 do not have reason to suspect that the mixing length
 560 for the low mass stars in the DR2 and ERD3 CMD is
 561 substantially lower than that of the sun we leave the
 562 investigation of these potential additionl uses for future
 563 work.

564 Finally, we do not find that the OPLIB opacity tables
 565 help in reproducing the as yet unexplained wedge shape
 566 of the observed Gap.

567

APPENDIX

568

A. PYTOPSSCRAPE

569 pyTOPSScrape provides an easy to use command line and python interface for the OPLIB opacity tables accessed
 570 through the TOPS web form. Extensive documentation of both the command line and programmatic interfaces is
 571 linked in the version controlled repository. However, here we provide a brief, illustrative, example of potential use.

572 Assuming pyTOPSScrape has been installed and given some working directory which contains a file describing a base
 573 composition (“comp.dat”) and another file containing a list of rescalings of that base composition (“rescalings.dat”)
 574 (both of these file formats are described in detail in the documentation), one can query OPLIB opacity tables and
 575 convert them to a form mimicking that of type 1 OPAL high temperature opacity tables using the following shell
 576 command.

577 \$ generateTOPStables comp.dat rescalings.dat -d ./TOPSCache -o out.opac -j 20

578 For further examples of pyTOPSScrape please visit the repository.

579

B. INTERPOLATING $\rho \rightarrow R$

580 OPLIB parameterizes κ_R as a function of mass density, temperature in keV, and composition. Type 1 OPAL high
 581 temperature opacity tables, which DSEP and many other stellar evolution programs use, instead parameterizes opacity
 582 as a function of temperature in Kelvin, R (Equation B1), and composition. The conversion from temperature in keV
 583 to Kelvin is trivial (Equation B2).

$$584 \quad 585 \quad 586 \quad R = \frac{\rho}{T_6^3} \quad (B1)$$

$$587 \quad 588 \quad T_K = T_{keV} * 11604525.0061657 \quad (B2)$$

589 However, the conversion from mass density to R is more involved. Because R is coupled with both mass density and
 590 temperature there there is no way to directly convert tabulated values of opacity reported in the OPLIB tables to their

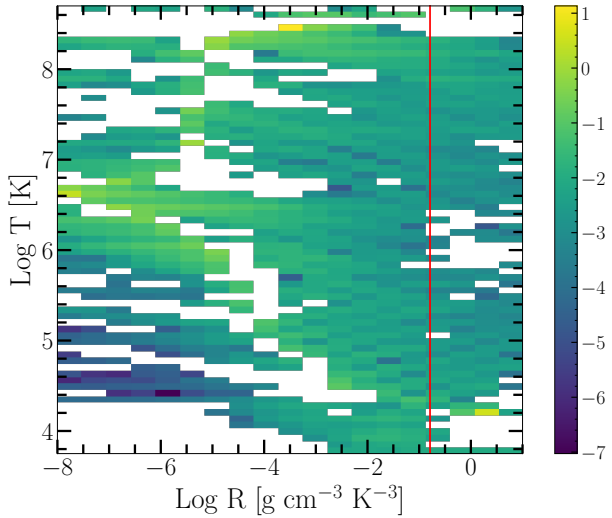


Figure 13. Log Fractional Difference between opacities in $\kappa_R(\rho, T_{eff})$ space directly queried from the OPLIB web-form and those which have been interpolated into $\log(R)$ space and back. Note that, due to the temperature grid of type 1 OPAL tables not aligning perfectly with the temperature grid OPLIB uses there may be edge effects where the interpolation is poorly constrained. The red line corresponds to $\log(R) = -0.79$ where much of a stellar model's radius exists.

equivalents in R space. The TOPS webform does allow for a density range to be specified at a specific temperature, which allows for R values to be directly specified. However, issuing a query to the TOPS webform for not just every composition in a Type 1 OPAL high temperature opacity table but also every temperature for every composition will increase the number of calls to the webform by a factor of 70. Therefore, instead of directly specifying R through the density range we choose to query tables over a broad temperature and density range and then rotate **these** tables, interpolating $\kappa_R(\rho, T_{eff}) \rightarrow \kappa_R(R, T_{eff})$.

To perform this rotation we use the `interp2d` function within `scipy's interpolate` (Virtanen et al. 2020) module to construct a cubic bivariate B-spline (Dierckx 1981) interpolating function s , with a smoothing factor of 0, representing the surface $\kappa_R(\rho, T_{eff})$. For each R^i and T_{eff}^j reported in type 1 OPAL tables, we evaluate Equation B1 to find

$$\rho^{ij} = \rho(T_{eff}^j, R^i). \text{ Opacities in } T_{eff}, R \text{ space are then inferred as } \kappa_R^{ij}(R^i, T_{eff}^j) = s(\rho^{ij}, T_{eff}^j).$$

As first-order validation of this interpolation scheme we can perform a similar interpolation in the opposite direction, rotating the tables back to $\kappa_R(\rho, T_{eff})$ and then comparing the initial, “raw”, opacities to those which have gone through the interpolations process. Figure 13 shows the fractional difference between the raw opacities and a set which have gone through this double interpolation. The red line denotes $\log(R) = -0.79$ where models **near the Jao Gap mass range** will tend to sit for much of their radius. Along the $\log(R) = -0.79$ line the mean fractional difference is $\langle \delta \rangle = 0.005$ with an uncertainty of $\sigma_{\langle \delta \rangle} = 0.013$. One point of note is that, because the initial rotation into $\log(R)$ space also reduces the domain of the opacity function, interpolation-edge effects which we avoid initially by extending the domain past what type 1 OPAL tables include cannot be avoided when interpolating back into ρ space.

This work has made use of the NASA astrophysical data system (ADS). We would like to thank Elisabeth Newton, Aaron Dotter, and Gregory Feiden for their support and for useful discussion related to the topic of this paper. We would like to thank our reviewer for their critical eye and their guidance to investigate to effects of the mixing length on the Gap Location. Additionally, we would like to thank James Colgan and the Los Alamos T-1 group for their assistance with the OPLIB opacity tables and support for the public release of `pyTOPSScrape`. We acknowledge the support of a NASA grant (No. 80NSSC18K0634).

Software: The Dartmouth Stellar Evolution Program (DSEP) (Dotter et al. 2008), `BeautifulSoup` (Richardson 2007), `mechanize` (Chandra & Varanasi 2015), `FreeEOS` (Irwin 2012), `pyTOPSScrape` (Boudreux 2022)

REFERENCES

- 618 Amard, L., Palacios, A., Charbonnel, C., et al. 2019, A&A,
 619 631, A77, doi: [10.1051/0004-6361/201935160](https://doi.org/10.1051/0004-6361/201935160)
- 620 Bahcall, J. N., Pinsonneault, M. H., & Basu, S. 2001, ApJ,
 621 555, 990, doi: [10.1086/321493](https://doi.org/10.1086/321493)
- 622 Bahcall, J. N., Serenelli, A. M., & Basu, S. 2005, ApJL,
 623 621, L85, doi: [10.1086/428929](https://doi.org/10.1086/428929)
- 624 Baraffe, I., & Chabrier, G. 2018, A&A, 619, A177,
 625 doi: [10.1051/0004-6361/201834062](https://doi.org/10.1051/0004-6361/201834062)
- 626 Baraffe, I., Chabrier, G., Allard, F., & Hauschildt, P. H.
 627 1997, A&A, 327, 1054.
<https://arxiv.org/abs/astro-ph/9704144>
- 628 Boudreault, T. 2022, tboudreault/pytopsscrape:
 629 pyTOPSScrape v1.0, v1.0, Zenodo,
 630 doi: [10.5281/zenodo.7094198](https://doi.org/10.5281/zenodo.7094198)
- 631 Chabrier, G., & Baraffe, I. 1997, A&A, 327, 1039.
<https://arxiv.org/abs/astro-ph/9704118>
- 632 Chandra, R. V., & Varanasi, B. S. 2015, Python requests
 633 essentials (Packt Publishing Ltd)
- 634 Choi, J., Dotter, A., Conroy, C., et al. 2016, ApJ, 823, 102,
 635 doi: [10.3847/0004-637X/823/2/102](https://doi.org/10.3847/0004-637X/823/2/102)
- 636 Colgan, J., Kilcrease, D. P., Magee, N. H., et al. 2016, in
 637 APS Meeting Abstracts, Vol. 2016, APS Division of
 638 Atomic, Molecular and Optical Physics Meeting
 639 Abstracts, D1.008
- 640 Creevey, O. L., Sordo, R., Pailler, F., et al. 2022, arXiv
 641 e-prints, arXiv:2206.05864.
<https://arxiv.org/abs/2206.05864>
- 642 Dierckx, P. 1981, IMA Journal of Numerical Analysis, 1,
 643 267, doi: [10.1093/imanum/1.3.267](https://doi.org/10.1093/imanum/1.3.267)
- 644 Dotter, A., Chaboyer, B., Jevremović, D., et al. 2008, The
 645 Astrophysical Journal Supplement Series, 178, 89
- 646 Feiden, G. A., Skidmore, K., & Jao, W.-C. 2021, ApJ, 907,
 647 53, doi: [10.3847/1538-4357/abcc03](https://doi.org/10.3847/1538-4357/abcc03)
- 648 Ferguson, J. W., Alexander, D. R., Allard, F., et al. 2005,
 649 ApJ, 623, 585, doi: [10.1086/428642](https://doi.org/10.1086/428642)
- 650 Fontes, C. J., Zhang, H. L., Abdallah, J., J., et al. 2015,
 651 Journal of Physics B Atomic Molecular Physics, 48,
 652 144014, doi: [10.1088/0953-4075/48/14/144014](https://doi.org/10.1088/0953-4075/48/14/144014)
- 653 Gaia Collaboration, Smart, R. L., Sarro, L. M., et al. 2021,
 654 A&A, 649, A6, doi: [10.1051/0004-6361/202039498](https://doi.org/10.1051/0004-6361/202039498)
- 655 Grevesse, N., & Sauval, A. J. 1998, SSRv, 85, 161,
 656 doi: [10.1023/A:1005161325181](https://doi.org/10.1023/A:1005161325181)
- 657 Hakel, P., Sherrill, M. E., Mazeved, S., et al. 2006, JQSRT,
 658 99, 265, doi: [10.1016/j.jqsrt.2005.04.007](https://doi.org/10.1016/j.jqsrt.2005.04.007)
- 659 Iglesias, C. A., & Rogers, F. J. 1996, ApJ, 464, 943,
 660 doi: [10.1086/177381](https://doi.org/10.1086/177381)
- 661 Irwin, A. W. 2012, FreeEOS: Equation of State for stellar
 662 interiors calculations, Astrophysics Source Code Library,
 663 record ascl:1211.002. <http://ascl.net/1211.002>
- 664 Jao, W.-C., & Feiden, G. A. 2020, AJ, 160, 102,
 665 doi: [10.3847/1538-3881/aba192](https://doi.org/10.3847/1538-3881/aba192)
- 666 —. 2021, Research Notes of the American Astronomical
 667 Society, 5, 124, doi: [10.3847/2515-5172/ac053a](https://doi.org/10.3847/2515-5172/ac053a)
- 668 Jao, W.-C., Henry, T. J., Gies, D. R., & Hambly, N. C.
 669 2018, ApJL, 861, L11, doi: [10.3847/2041-8213/aacdf6](https://doi.org/10.3847/2041-8213/aacdf6)
- 670 Jermyn, A. S., Bauer, E. B., Schwab, J., et al. 2022, arXiv
 671 e-prints, arXiv:2208.03651.
<https://arxiv.org/abs/2208.03651>
- 672 Joyce, M., & Chaboyer, B. 2018, ApJ, 864, 99,
 673 doi: [10.3847/1538-4357/aad464](https://doi.org/10.3847/1538-4357/aad464)
- 674 MacDonald, J., & Gizis, J. 2018, MNRAS, 480, 1711,
 675 doi: [10.1093/mnras/sty1888](https://doi.org/10.1093/mnras/sty1888)
- 676 Magee, N. H., Abdallah, J., Colgan, J., et al. 2004, in
 677 American Institute of Physics Conference Series, Vol.
 678 730, Atomic Processes in Plasmas: 14th APS Topical
 679 Conference on Atomic Processes in Plasmas, ed. J. S.
 680 Cohen, D. P. Kilcrease, & S. Mazavet, 168–179,
 681 doi: [10.1063/1.1824868](https://doi.org/10.1063/1.1824868)
- 682 Mansfield, S., & Kroupa, P. 2021, A&A, 650, A184,
 683 doi: [10.1051/0004-6361/202140536](https://doi.org/10.1051/0004-6361/202140536)
- 684 Nutzman, P., & Charbonneau, D. 2008, PASP, 120, 317,
 685 doi: [10.1086/533420](https://doi.org/10.1086/533420)
- 686 Richardson, L. 2007, April
- 687 Rodríguez-López, C. 2019, Frontiers in Astronomy and
 688 Space Sciences, 6, 76, doi: [10.3389/fspas.2019.00076](https://doi.org/10.3389/fspas.2019.00076)
- 689 Seaton, M. J., Yan, Y., Mihalas, D., & Pradhan, A. K.
 690 1994, MNRAS, 266, 805, doi: [10.1093/mnras/266.4.805](https://doi.org/10.1093/mnras/266.4.805)
- 691 Skrutskie, M. F., Cutri, R. M., Stiening, R., et al. 2006, AJ,
 692 131, 1163, doi: [10.1086/498708](https://doi.org/10.1086/498708)
- 693 Sollima, A. 2019, Monthly Notices of the Royal
 694 Astronomical Society, 489, 2377,
 695 doi: [10.1093/mnras/stz2093](https://doi.org/10.1093/mnras/stz2093)
- 696 Spada, F., Demarque, P., & Kupka, F. 2021, MNRAS, 504,
 697 3128, doi: [10.1093/mnras/stab1106](https://doi.org/10.1093/mnras/stab1106)
- 698 Trampedach, R., Stein, R. F., Christensen-Dalsgaard, J.,
 699 Nordlund, Å., & Asplund, M. 2014, MNRAS, 445, 4366,
 700 doi: [10.1093/mnras/stu2084](https://doi.org/10.1093/mnras/stu2084)
- 701 van Saders, J. L., & Pinsonneault, M. H. 2012, ApJ, 751,
 702 98, doi: [10.1088/0004-637X/751/2/98](https://doi.org/10.1088/0004-637X/751/2/98)
- 703 Virtanen, P., Gommers, R., Oliphant, T. E., et al. 2020,
 704 Nature Methods, 17, 261, doi: [10.1038/s41592-019-0686-2](https://doi.org/10.1038/s41592-019-0686-2)